QIRT 10 10th International Conference on Quantitative InfraRed Thermography
July 27-30, 2010, Québec (Canada)

Quantitative assessment of the improvement of the detection of defects by pulse thermography thanks to the TSR approach in the case of a smart composite repair patch

by D. L. Balageas, B. Chapuis, G. Deban, F. Passilly

ONERA, Dept. of Composite Materials and Structures, BP 72, 92322 Châtillon, France - daniel.balageas@onera.fr

Abstract

The work aims to assess quantitatively the improvement given by using the Thermographic Signal Reconstruction (TSR) approach to the detectivity of defects in structures. The considered structure is a smart composite repair patch used in aeronautics. Artificial defects simulating a debond at the patch/structure interface are to be detected. The signal to noise ratio of the defect in the sound structure background is calculated as an index of detectivity. A strategy is proposed for optimizing the time of observation allowing the best detection and characterization.

1. Introduction

The TSR (Thermographic Signal Reconstruction) method proposed by Shepard [1-4], is well known and largely used in Non-Destructive Evaluation. The method, used for pulsed stimulated thermographic experiments, consists in:

- The fitting of the experimental log-log plot thermogram by a logarithmic polynomial:

$$\ln(\Delta T) = a_0 + a_1 \ln(t) + a_2 [\ln(t)]^2 \ldots + a_n [\ln(t)]^n \quad (1)$$

This fitting is particularly well suited for pulse heating. It is sometimes called Logarithmic Fitting Adiabatic (LFA).

- The replacement of the sequence of temperature increase images, $\Delta T(i,j,t)$, by the series of $(n+1)$ images of the polynomial coefficients: $a_0(i,j)$, … $a_n(i,j)$. This operation allows a drastic reduction of the data amount. From this series of $(n+1)$ images it is then possible to reconstruct the full sequence of the experiment.

- The use for NDE purpose of the second derivative of the thermogram, $d^2 \ln(\Delta T / \Delta T_\infty) / d \ln(Fo)^2$, the derivation being achieved directly on the polynomial, then without increase of the temporal noise. The derivations present the advantage of producing a normalization leading to images unaffected by a non-uniform illumination or a non-uniform absorptivity.

- The improvement of the detection of defects by increasing the contrast between sound and defective areas and the reducing the blurring due to 3-D thermal diffusion effects thanks to a possible earlier detection of the contrast.

Despite an abundant literature, until now the use of the TSR technique remains relatively qualitative, if we except recent papers from Shepard [3,4]. The situation is explicable since most of the applications of the method deal with NDE (Non Destructive Evaluation) problems for which excellent detection performances are more important than precise properties measurements. In such a context, this work, similarly to the one presented in a companion paper [5] on application of the TSR technique to front-face pulse diffusivity measurement, want, to be resolutely quantitative.

We chose to apply the TSR technique to a complex structure representative of practical applications: a smart composite repair patch instrumented with piezoelectric transducers, bonded on an aluminum plate. This type of smart repair can be used in both civil engineering and aerospace fields [6].

2. Tested structure

Fig. 1 presents the tested coupons. The thermographic NDE test aims to detect possible debonds at the patch/substructure interface and could be used as a validation of the repair at the end of the repair process. To judge of the detectivity of the thermographic NDE, several artificial defects have been introduced in such coupons. Each coupon contains only one defect. These defects are the followings: i) a 14 mm-dia. hole in the aluminum plate (simulating a severe debond with air inclusion (infinite thermal resistance), ii) a Teflon disc-shaped insert, 15 mm in dia., and 20 μm -thick, iii) a pre-polymerized bond insert,15 mm in dia., 300 μm-thick, instead of the normal bond layer. These defects are located in a sound area of the patch and not in the vicinity of the piezoelectric transducers. These transducers can be used to detect interface defects in their close vicinity using the electro-impedance technique, completing in this way the thermographic NDE for the validation of the repair. After the validation of the repair, these piezoelectric inserts monitor the repaired structure using the acousto-ultrasonic technique (Lamb waves).

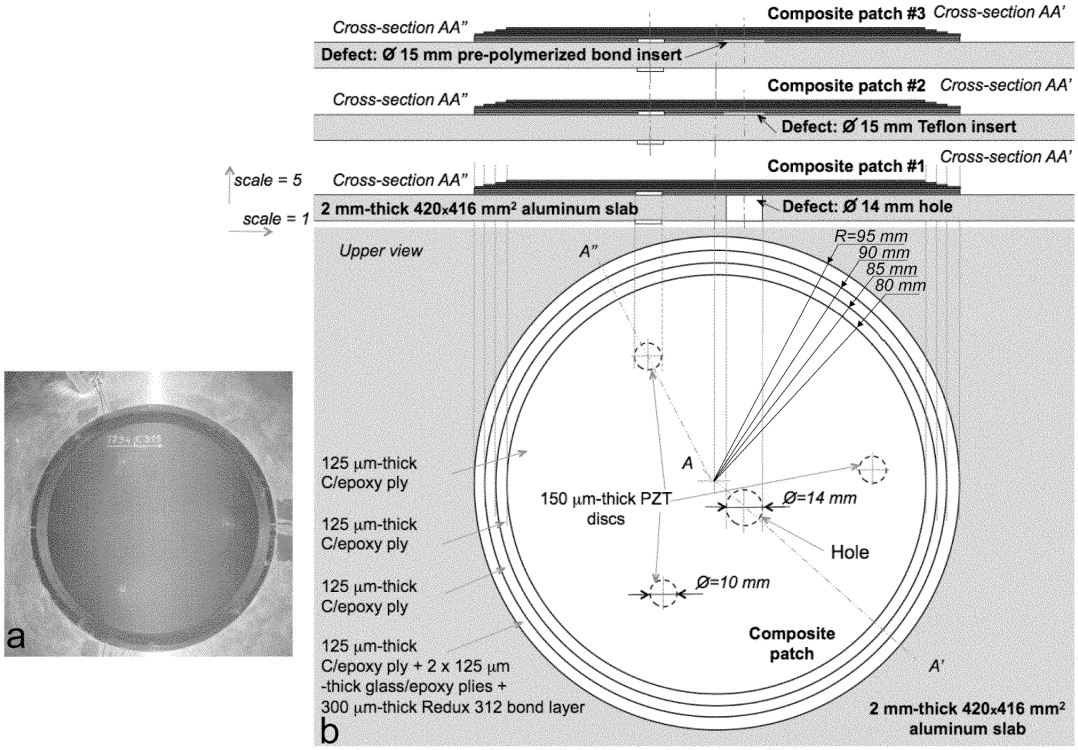

Figure 1. *a) Smart composite repair patch with the three tested artificial defects. Here, each embedded PZT transducer is accompanied by a second one bonded on the aluminum plate rear-face, for an easy selection of Lamb wave modes. In a real situation the second PZT disc is not present. – b) Photo of a coupon (patch bonded on an aluminum plate).*

3. Method for evaluating the defect detectivity

To characterize quantitatively the detectivity of the method, we calculate for the thermogram, $\Delta T(t)$ (normalized and then fitted by a logarithmic polynomial), and the 1st and 2nd logarithmic derivatives, a signal to *noise* ratio of the defect, $(S/N)_d$, defined as the ratio of the absolute value of the absolute contrast of these parameters between the defective and the sound zones ($|C_d|$) to the scatter of the related parameters in the sound zone. The definition of the areas that can be considered as sound is not obvious since the infrared images reveal that the regions surrounding the piezoelectric transducers are slightly different from distant regions (see Fig. 2). This is due to the fact that these transducers are bonded to the composite patch and the aluminum plate by extra bond layers that are more extended than the piezoelectric discs and that there is for electric purpose a sheet of Kapton of 12 μm thickness inserted between the PZT and the aluminum. The existence of these extra materials produces a time behavior of the temperature in these regions that is characterized by a delay in the occurrence of the composite/aluminum transition zone. Consequently, the scatters (σ_s) of the sound areas are taken equal to the standard deviations of the parameters ($\Delta T(t)$, and the 1st and 2nd logarithmic derivatives) calculated from 16 different pixels chosen in the sound zone, as far as possible from the vicinities of the piezoelectric transducers (see the example given in Fig. 3a). The defect contrast for the thermograms, $\Delta T(t)$, is taken as the difference between the temperature increase in the central part of the defect, ΔT_d, and the mean value of the temperature increases of the 16 points taken as reference for the sound region, $\Delta T_{s_{means}}$. The resulting detectivity, defined as the signal-to-noise ratio of the defect is:

$$(S/N)_d = |C_d| / \sigma_s = |\Delta T_d - \Delta T_{s_{means}}| / \sigma_s$$

Detectivities are similarly calculated for the first and the second derivatives of the logarithmic temperature increases.

4. Evaluation of the defect detectivity in the case of the first defect (hole)

The method for evaluating the detectivity of the defects has been applied in the case of the three artificial defects. A detailed analysis of the results is given in the present section and in section 5 for the first artificial defect (a hole machined in the aluminum plate). Section 6 will give only synthetic results on the defect detectivity for the two others defects.

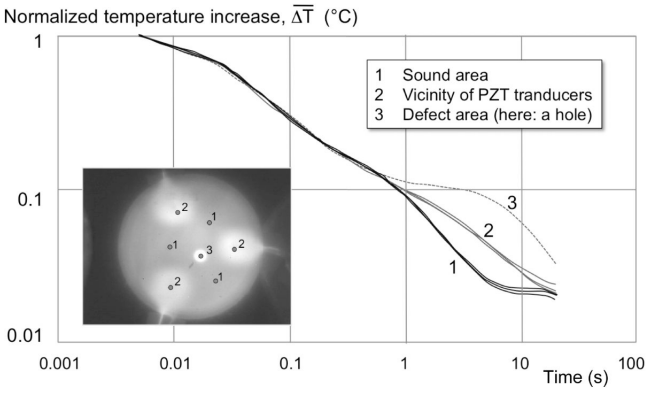

Figure 2. *Compared behavior of the sound area of the patch (1), the vicinity of the piezoelectric transducers (2), and a defective area (in this example a hole in the aluminum plate). The normalization consists in dividing each thermographic image by the first image following the pulsed stimulation. The thermograms are fitted by a polynomial of degree 9.*

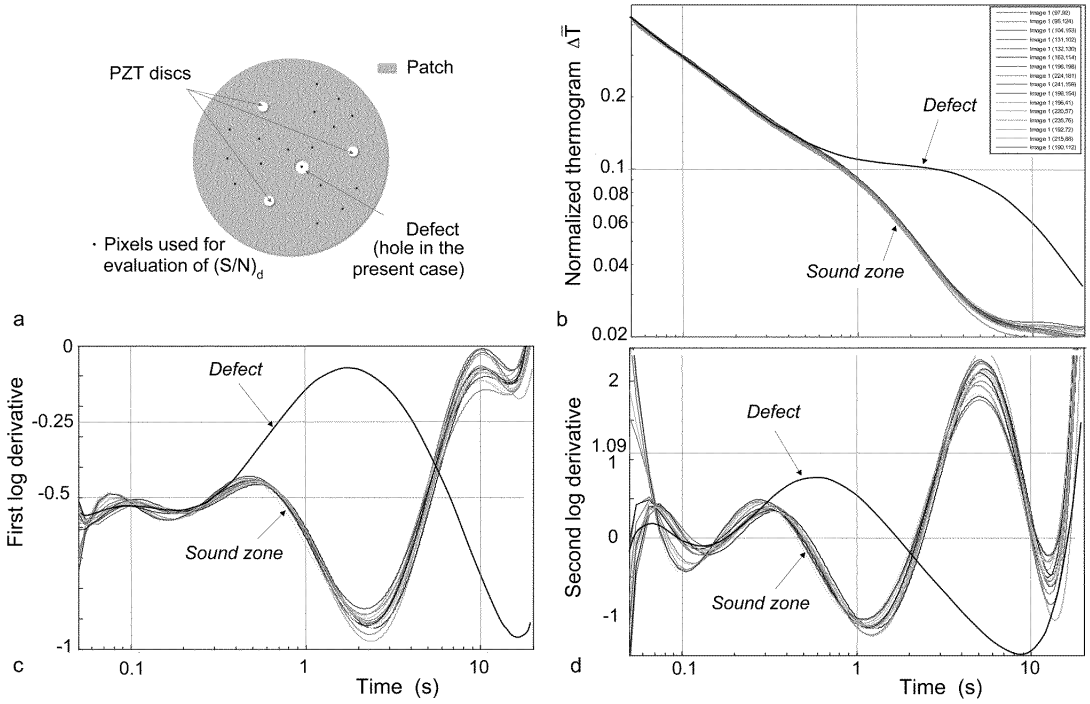

Figure 3. *a) The 16 pixels of the sound region used for the evaluation of the $(S/B)_d$; b) Normalized thermograms fitted by a logarithmic polynomial of degree 9 (TSR method); c and d) idem 1st and 2nd logarithmic derivatives.*

Fig. 3 presents the logarithmic polynomial fitting of the normalized thermograms and their 1st and 2nd derivatives for the 16 points of the sound zone and of the central part of the defective area. The thermograms of the sound region present a scatter that increases with time, is amplified by the derivations, and is due to the spatial variability of the composite and of the bond. The contrast between the defective zone and the sound region begins after a few tenths of second and increases up to a maximum occurring for a few seconds. Both the scatter σ_s and the contrast, C_d, for the three parameters ($\Delta T(t)$, 1st and 2nd logarithmic derivatives) vary independently with time as seen in Fig. 3. The resulting detectivities, $(S/N)_d = | C_d | / \sigma_s$, follow rather complicated evolution laws characteristic of the properties and geometry of the components of the structure and of the nature of the defect. As shown in Fig. 4, the values and times of occurrence of the extremums of the detectivities are very different for the three parameters ($\Delta T(t)$, 1st and 2nd derivatives). The marks **+** and **–** indicate when the contrast is positive and negative. These detectivities obtained by the TSR method are compared to those of the crude thermogram and of the thermogram filtered by a low-pass filter available in the Cedip ALTAIR software. The last two detectivity curves are near of the one corresponding to the thermogram fitted by a logarithmic thermogram, but they suffer of an important noise.

The comparison between the 3 curves given by the TSR method shows that the higher detectivity ($(S/N)_d$ = 90) is obtained using the thermogram and not the derivatives. Nevertheless, this high detectivity is obtained for times higher than 2 s, and for shorter times is strongly weaker than that given by the derivatives. Thus, for [0.3 s - 2 s], the derivations enhances the detectivity by a factor of 2 to 7, yet it is in this time domain that we can find the useful information related to depths corresponding to the patch/

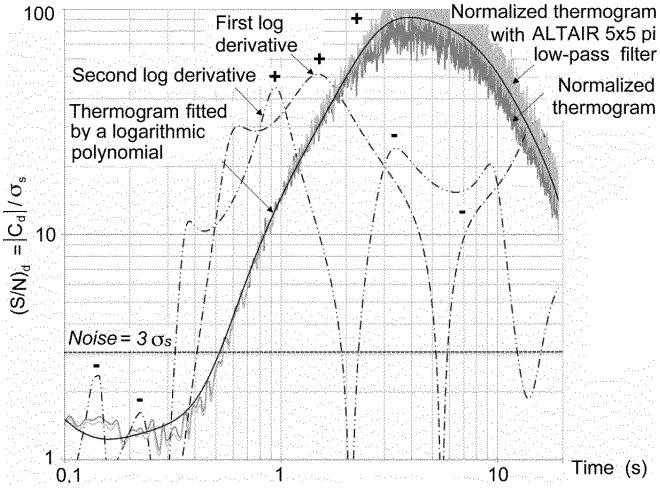

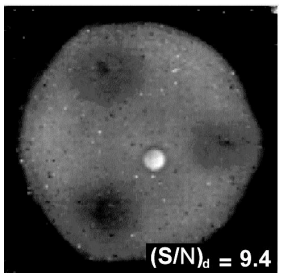

Figure 4. *Left: $(S/N)_d$ ratios for the fitted thermograms and their derivatives. Compa-rison to the $(S/N)_d$ corresponding to the direct exploitation of the normalized thermograms. Right top: the best image of the defect, obtained at t=0,355 s (1st peak of 2nd derivative).*

structure interface to characterize. The high detectivity obtained with the thermogram is not interesting since images are too much influenced by the metallic structure and blurred by 3-D conduction effects producing a loss of space resolution (Fig. 5). We see that building an identification strategy based on the only maximization of the contrast, C_d, or the detectivity, $(S/N)_d$, leads to a deadlock. On the contrary, an optimization based on both a good detectivity and a very early characterization is highly preferable. Here, the best moments for the defect detection/identification are near 0.35 s for the 2nd derivative and near 0.6 s for the 1stderivative. These times correspond to a very early detection and are far from the occurrence times of the maximum contrasts shown in Fig. 3c-d.

Fig. 5 presents an overview of the thermographic images taken at the occurrence times of the maximums of $(S/N)_d$. The following images are compared: crude normalized thermograms, normalized thermograms fitted by the logarithmic polynomial, 1st and 2nd logarithmic derivatives. All images show the circular areas surrounding the piezoelectric transducers (see explanation in section 3). We will focus our attention on the defect zone, in the center of the patch. There, we notice:

- the fidelity to the original images of the images fitted by the logarithmic polynomial. This quality of the fitting can be quantified by the correlation coefficient, R^2. Fig. 6 presents the distribution of this coefficient for two values of the degree of the fitting polynomial: 7 and 9. The higher degree leads to higher R^2 and has been chosen. It is interesting to notice that the distribution of R^2 produces an image allowing the detection of the defect.
- for the shorter time (0.355 s), no detection of the defect from the thermogram images and the beneficial influence of the two derivations that makes the defects visible, allowing a very early detection that leads to a defect image with no lateral conduction effect. The so-obtained image of the defect is the best image among the full collection presented in Fig. 5.
- for the following times, the permanence of the defect image, which remains visible up to the end of the test (20 s). This is due to the nature of the artificial defect and is not representative of what would occur with a real defect affecting only the patch/structure interface. For almost anytime the defect contrasts of the derivatives are better than hose of the thermograms.
- that when time increases, the blurring become more and more pronounced, impeding to measure the exact extent of the defect. Furthermore, this increase of the loss of spatial resolution is more pronounced for the derivatives. This leads to the following important conclusion that to optimally exploit the TSR technique, it is recommended using the early detection strategy.

5. Quantitative analysis of the thermograms and of their derivatives in the case of the first defect (hole)

The hole machined in the Al plate and in the bond layer is equivalent to a defect with an infinite thermal resistance. Furthermore, when considering the early contrast, the heat field in the coupon as really 1-D. In these conditions, the relation given by Ref. [7], between the early relative contrast, Cr_d the depth of the defect, and the diffusivity of the material between the upper patch surface and the defect (CFRP and GFRP layers), can be applied with the knowledge of the defect depth equal to the total thickness of the composite plies, L, permitting to calculate the mean diffusivity of the composite patch, $\overline{\alpha}$:

$$\overline{\alpha} = L^2 \Big/ \left[t \, Ln(2 / Cr_d(t)) \right]. \qquad (2)$$

Knowing the total thickness of the composite layers (L = 750 μm), the formula (2) gives, for instance at t = 0.8 s, with a relative contrast calculated from the fitted thermograms equal to 14.5%, a mean diffusivity $\overline{\alpha}$ = 2.64 10^{-7} m^2s^{-1}. This so-identified diffusivity, for the time domain [0.57s-1.17s] is quasi constant (at ± 5%), although the relative contrast varies between 6% and 35%. So, to verify the quality of the TSR approach, we can compare this calculated value to the mean diffusivity of the composite patch estimated by another way. Starting from diffusivities, specific heats and thicknesses of the two composites given in the literature (see Table 1), it is possible to calculate the equivalent mean thermal conductivity and mean heat capacity of this plies stack (see Fig. 1), and finally to evaluate its equivalent diffusivity: 2.62 10^{-7} m^2s^{-1}, a value in very good agreement with the value identified above from the contrast of the fitted thermograms.

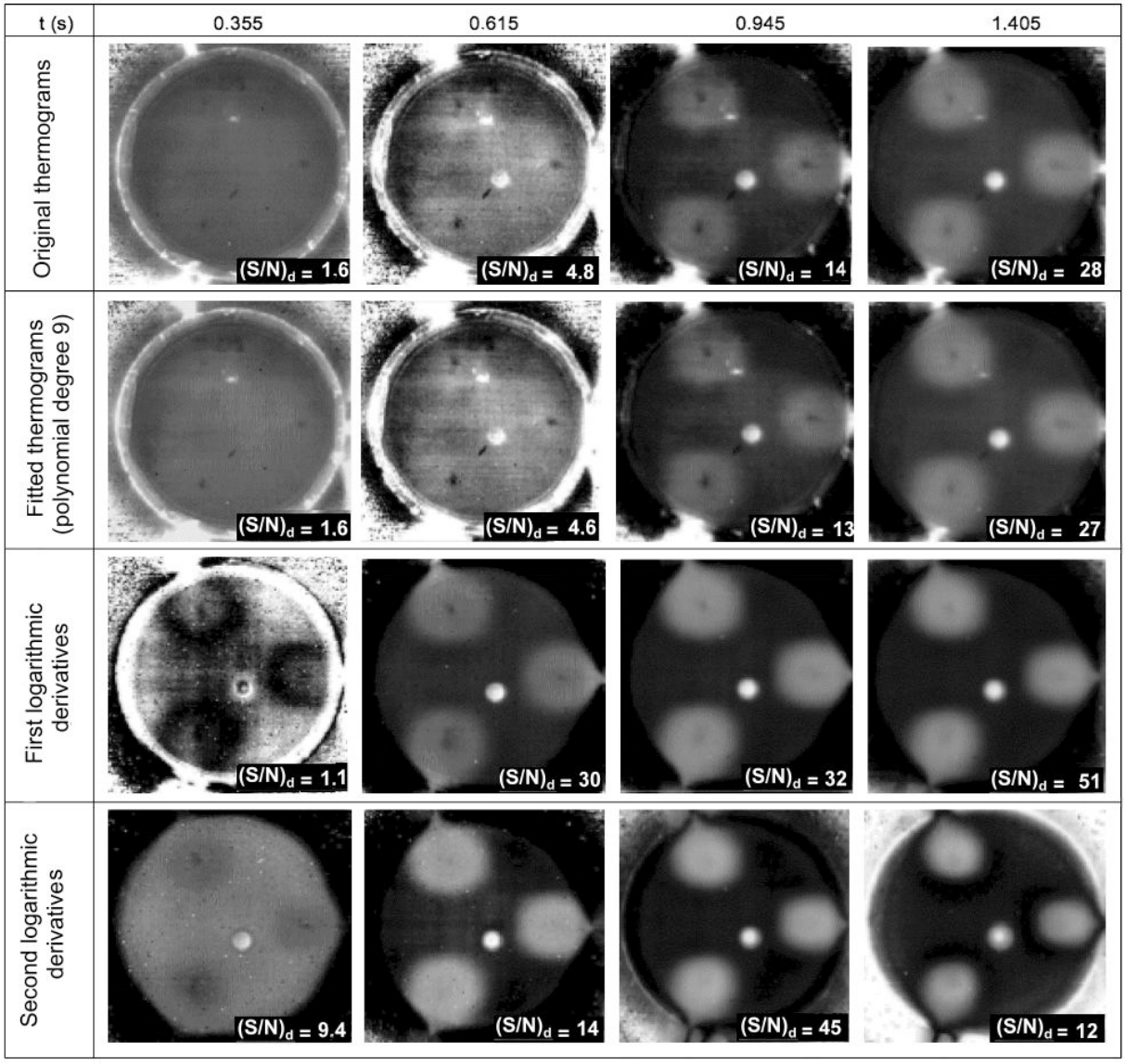

Figure 5. *Comparison of the thermographic images obtained by the TSR technique for the times corresponding to the occurrence of the maximums of detectivity.*

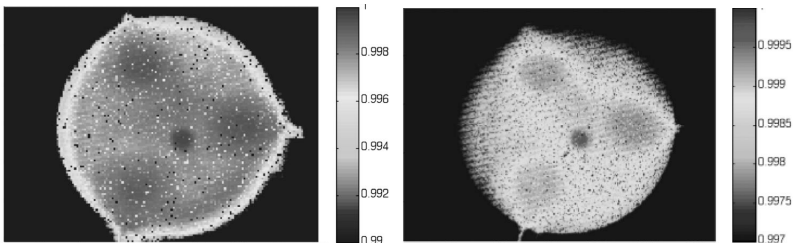

Figure 6. *The fidelity of the fitting quantified by the correlation coefficient R^2. Left: images of R^2 for a polynomial of degree 7, with R^2 on the coupon >0.994; right: idem, for a polynomial of degree 9, with R^2 on the coupon >0.997.*

For evaluating the mean diffusivity of the composite patch it is also possible to use the characteristic time t^* for which the first derivative is equal to -0.25, the theoretical half-rise value (see [5]). We find (see Figure 3c): t^* = 0.70 s, which leads to:

$$\bar{\alpha} = L^2/\pi\, t^* = 2.56\ 10^{-7}\ m^2s^{-1}, \quad (3)$$

a value in very good agreement with those found from the thermogram (the difference is 3%). The time t^* can be also deduced from the second derivative, corresponding to the first maximum of this function, here equal to 0.605 s, which leads to a higher estimate of 2.96 10^{-7} m^2s^{-1}, using the same formula (3). The coherent values of the patch diffusivity evaluated by these different ways, presented in Table 2, validate quantitatively the TSR approach, at least the use of the first derivative.

Table 1. *Thermal properties of the materials constituting the coupon, evaluated from the literature, and of the material equivalent to the mixed composite (CFRP plies plus GFRP plies).*

Material	Diffusivity $m^2 s^{-1}$	Vol. specific heat $J\ m^{-3}K^{-1}$	Conductivity $W\ m^{-1}\ K^{-1}$	Characteristic length (m)	Diffusion time $t^*=L^2/\pi\alpha$
C/epoxy	3.13E-07	1.92E+06	6.00E-01	5.00E-04	2.54E-01
Glass/époxy	2.13E-07	1.55E+06	3.30E-01	2.50E-04	9,34E-02
Redux 312	1.70E-07	1.50E+06	2.50E-01	3.00E-04	1.69E-01
Aluminum	1.03E-04	2.43E+06	2.50E+02	2.00E-03	1.24E-02
Equivalent composite	2.62E-07	1.80E+06	4.72E-01	7.50E-04	6.83E-01

Table 2. *Comparison between the a priori estimated patch diffusivity and the values deduced from TRS approach.*

Way to estimate the patch diffusivity	Diffusivity (m^2s^{-1})
Estimation from the literature (see table 1)	2.62 10^{-7}
Experimentally, from the early contrast of the thermogram	2.64 10^{-7}
Experimentally, from the half-rise of the 1st derivative	2.56 10^{-7}
Experimentally, from the first maximum of the 2ndderivative	2.96 10^{-7}

6. Evaluation of the defect detectivity in the case of the other two artificial defects

As shown in Fig. 1, other artificial defects have been manufactured in two other coupons for which pulsed thermography and TSR technique have been similarly applied. The detectivity of the defects has been also studied.

6.1. Repair patch with an insert of pre-polymerized bond (Redux 312)

The fitted thermogram and its log derivatives are presented in Fig. 7 (first row). The sound zone is described by 14 different pixels (grey curves) and the defect by a unique pixel chosen in its central part (curve in black). The contrasts are weaker compared to those obtained with the hole (Fig. 3) and the standard deviation for the sound zone smaller. This last fact increases the detectivity, but the quantitative value of this parameter is not precise since from one coupon to the other the pixels chosen are not exactly the same. The $(S/N)_d$ curves are presented in Fig. 8-left.

The detectivity of the pre-polymerized bond insert, using the thermograms is lower than 18, which is more than 5 times less than the detectivity of the hole. Furthermore, it decreases more rapidly for times larger than 10 s. This is due to the fact that the defect is just located at the interface and not affecting the metallic structure as the hole in the previous case. The detectivities of the derivatives present more complicated evolutions and the second derivative detectivity is noticeably higher (peaking at values higher than 100 at the early time of 0.3 s). The use of derivatives, and particularly the second derivative allows a substantial enhancement of the detectivity in the present case.

The best image of the defect is obtained for t=0.6 s with the 1st derivative. This image (Fig. 9) is far better than the best ΔT image (obtained for t=2.2 s). It appears that next to the circular artificial defect three other smallest defects exist in between it and one of the piezoelectric transducers. Their nature is unknown and will be discovered at the end of the study (still in progress) by a post-mortem analysis. An ultrasonic attenuation image has been obtained which corroborates the thermographic image (Fig. 9d). Finally the 2nd derivative image at 0.2 s is also given. It is remarkable that the use of the TSR technique produces an image of the unexpected defects better than that produced by ultrasounds.

The details in the piezo zones are also visible on the themographic images, although here the ultrasounds are better. Finally, the 2nd derivative at the very earlier time (0.2 s), in spite of the high $(S/N)_d$ does not give the better image of the defects. This is normal since at so earlier a time the information is mostly coming from the first plies of the composite. This produces rectangular patterns also seen in the ultrasonic image.

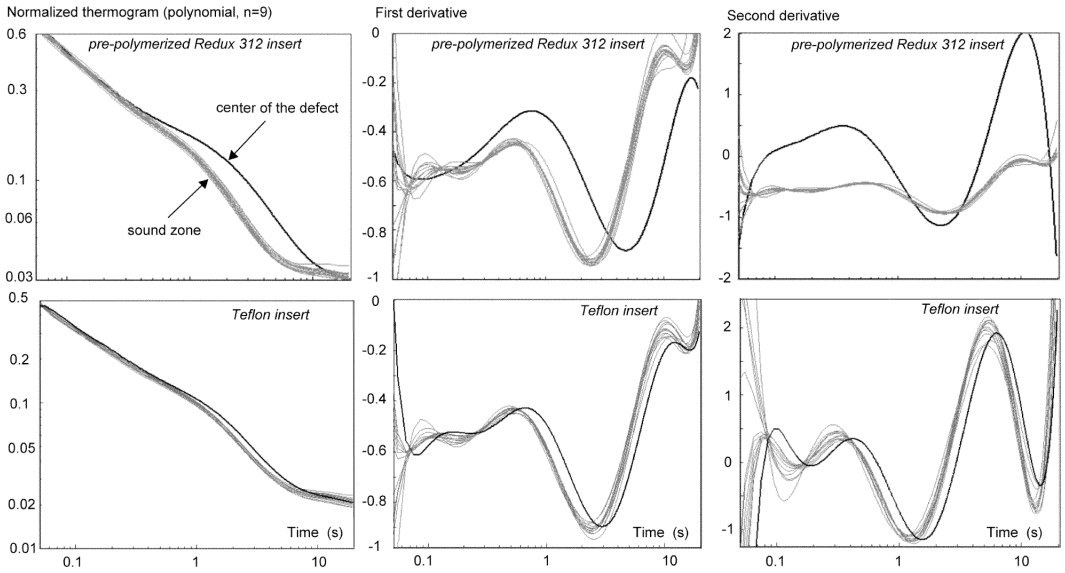

Figure 7. *Normalized thermograms (logarithmic polynomial of degree 9) (left), 1st (center) and 2nd (right) logarithmic derivatives. Comparison between sound and defective regions for pre-polymerized bond insert (1st row) and Teflon insert (2nd row).*

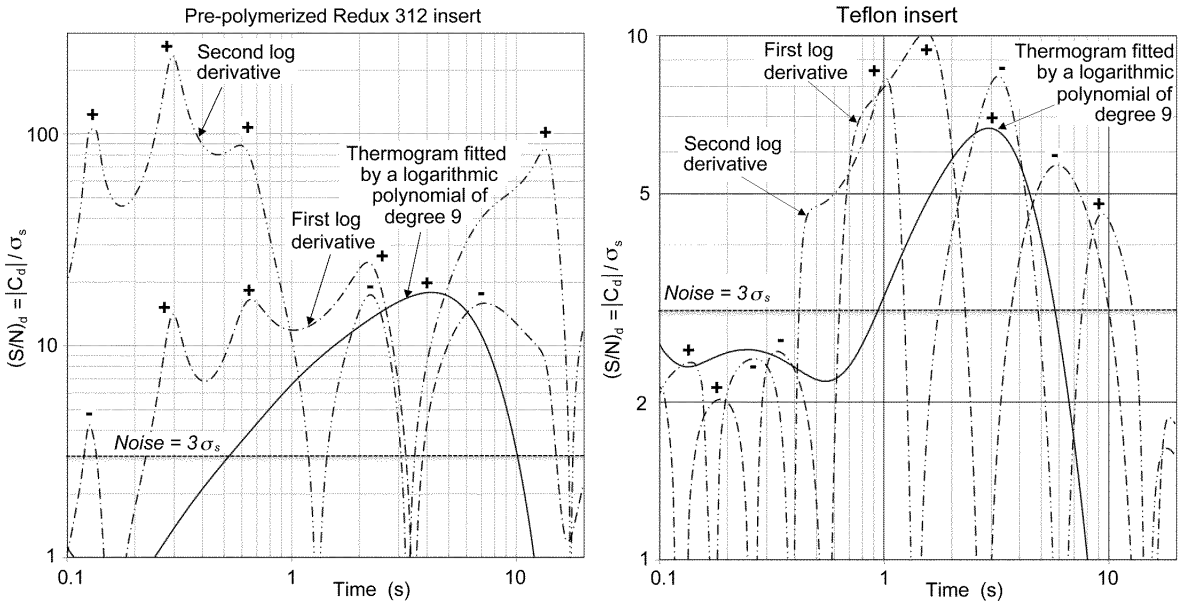

Figure 8. *$(S/N)_d$ ratios for the fitted thermograms and their derivatives. Left: pre-polymerized bond insert; right: Teflon insert. The (+) or (-) signs indicates if the contrast is respectively positive or negative.*

6.2. Repair patch with an insert of Teflon

Fig. 7 presents the fitted thermogram and its log derivatives. The sound zone is described by 12 different pixels (grey curves) and the defect by a pixel of its central part (curve in black). The contrasts are weak compared to those obtained with the hole (Fig. 3) and even to the pre-polymerized bond insert. This is rather unexpected since the Teflon diffusivity is 1.3 10^{-7} m^2s^{-1}, lower than that of the bond. This could be due to differences in the quality of the insert/composite and insert/Al interfaces. The corresponding *$(S/N)_d$* curves are presented in Fig. 8-left. The detectivity of the Teflon insert, using the thermograms is lower than 7, more than 10 times less than the detectivity of the hole. Furthermore, the level of the ΔT from the very beginning is higher than the mean value of the sound zone (apparent contrast: 2.5 σ_s). This situation impedes a detection before 1 s, a value higher than the characteristic time *t** of the composite layers (Table 1) and far from an early detection times.

The 1st and 2nd log derivatives improve the detection: respectively for the 1st and 2nd derivatives, an early detection is possible as soon as 0.6 and 0.4 s with detectivities equal to 7 and 4.5. The maximum detectivity obtained with the 1st derivative at 1.5 s is higher than 10. In the period [0.4 s – 1.5 s] the derivations enhance the detectivity by a factor near of 3. At any time, the detectivity using the derivatives is better than the one obtained using the ΔT *(see Fig. 10)*.

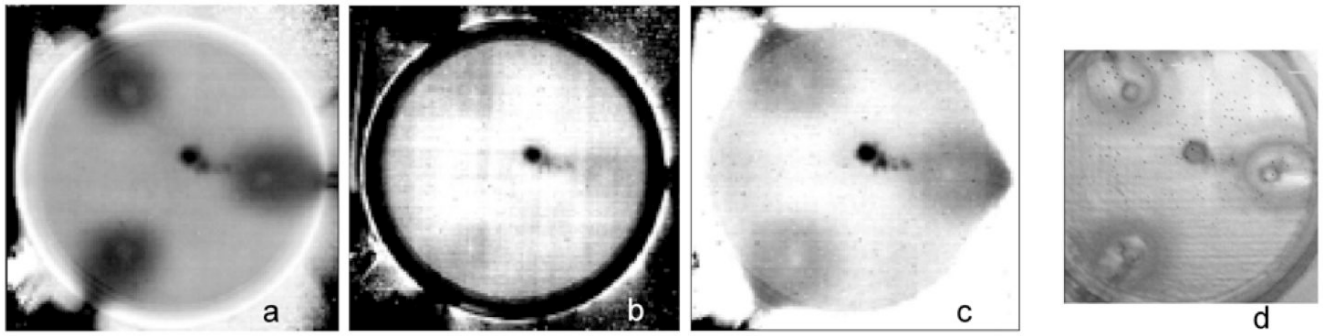

Figure 9. *Sample with the Redux 312 insert: a) ΔT at 2.20 s; b) 2nd derivative at 0.20 s; c) 1st derivative at 0.6 s; d) ultrasonic absorption image. The thermographic images are presented with an inversed grey scale to be comparable to the ultrasonic image.*

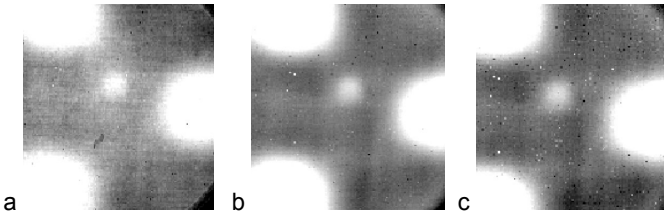

Figure 10. *Sample with the Teflon insert: ΔT (a), 1st derivative (b) and 2nd derivative (c) best defect images, respectively taken at 1.6 s, 1.6 s and 1s*

7. Conclusion

The TSR method was applied to the detection of artificial defects at the interface between a structure and a composite repair patch. The defect detectivity has been quantified, showing: i) a reduction of the temporal noise, ii) an improvement of the visual detection thanks to the logarithmic derivations, iii) an improvement of the precociousness of the defect detection, which is of prime importance for the quantitative characterization of the defects (depth, extent). These points have been verified for weak, mild, and very severe defects. So the interest of the TSR method is here quantitatively confirmed.

From a more general point of view, the study demonstrates the importance of evaluating not only the value of the detectivity for the maximum of the contrast, but also how it is important to study the detectivity-time evolution for an effective improvement of both the detection and the characterization of defects. A good strategy for optimizing the interpretation of thermographic NDE tests must begin by the evaluation of this time history of the detectivity, easily calculated from the experiment. It has been demonstrated that a smart use of the TSR approach can make the quality of thermographic images comparable to that of ultrasonics.

REFERENCES

[1] Shepard S.M., Ahmed T., Rubadeux B.A., Wang D., Lhota J.R., Synthetic processing of pulsed thermographic data for inspection of turbine components, *Insight,* Vol. 43, No 9, Sept. 2001, pp. 587-589.

[2] Shepard S.M., "Flash Thermography of Aerospace Composites ", *4th Pan American Conf. for NDT*, Oct. 2007, Buenos Aires, Argentina - http://www.ndt.net/article/ panndt2007/papers/132.pdf

[3] Shepard S.M., Hou J., Lhota J.R., Golden J.M., "Automated processing of thermographic derivatives for quality assurance", *Opt. Eng.* Vol. 46, No 5, May 2007.

[4] Shepard S.M., Lhota J.R., Ahmed T., "Measurement limits in flash thermography", SPIE Thermosense XXXIth Conference, *Proc. SPIE Conf. Vol. 7299*, 2009.

[5] Balageas D., Thickness or diffusivity measurements from front-face flash experiments using the TSR (thermographic signal reconstruction) approach, QIRT 2010, Proceedings, July 2010, Quebec, QC, Canada.

[6] Chapuis B., Terrien N., Royer D., Déom A., Smart composite repairs using PZT discs as actuators/sensors, *Structural Health Monitoring 2008*, DEStech Publ. Inc., pp. 665-672.

[7] Krapez J.-C., Balageas D., Déom A., Lepoutre F., "Early detection by stimulated infrared thermography", *Advances in Signal Processing for Nondestructive Evaluation of Materials,* X.V. Maldague Ed., Kluwer Acad. Publ., 1994, pp. 303-321.